

3-D Moderator Circulation Simulation of CANDU6 Nuclear Reactor Using CFX-4.3

C. Yoon, B.W. Rhee, and B.J. Min

Korea Atomic Energy Research Institute
150 Dukjin-dong Yusung-ku, Taejon 305-353, Korea

Abstract

3D CFD simulation for predicting the local subcooling of the moderator in the vicinity of the calandria tubes in a CANDU6 reactor is performed. For the current simulation, a set of grid structures with the same geometry as the Wolsong unit 2/3/4 moderator tank, called calandria, is generated and the momentum, heat and continuity equations are solved by CFX-4.3, a CFD code developed by AEA technology. The standard k- ϵ turbulence model associated with logarithmic wall treatment and SIMPLEC algorithm on the body fitted grid are used and Buoyancy effects are accounted for by the Boussinesq approximation. For the operating condition simulated in this study (103% full power), the flow pattern identified is the Buoyancy-dominated flow, which is generated by the interaction between the dominant Buoyancy force by heating and inertial momentum forces by the inlet jets. As a result, the velocity field and temperature distribution of a CANDU6 moderator in the operating condition are presented. The maximum temperature of the moderator is 90.3 °C, and the circulation pattern is reasonable.

1. Introduction

For some loss of coolant accidents with coincident loss of emergency core cooling in the CANDU reactor(Fig. 1), fuel channel integrity depends on the capability of the moderator to act as the ultimate heat sink, which is determined by moderator subcooling. Higher moderator temperatures (lower subcooling) would decrease the margin of the calandria tubes to dryout in the event that a pressure tube contacts the calandria tube due to local heating of the pressure tubes. As a preliminary study before the transient simulation of the CANDU moderator system on these accidents, a steady-state moderator behavior for 103% full power is analyzed in the current simulation.

In 1983, Koroyannaski, et al. [1] experimentally investigated the flow phenomena generated by the inlet jet and internal heating of a fluid in a Calandria-like cylindrical vessel, which was called 'SPEL experiments' because the facility was built in Sheridan Park Engineering Laboratory. A chemical flow visualization technique was employed to determine the predominant flow regime inside the vessel. Detailed temperature profiles inside the vessel were obtained using an optical fibre probe. These experimental results give an intuitional observation on the relationship between the moderator circulation pattern and the inlet flow rate and heat load.

In 1995, Collins [2] performed a moderator circulation analysis for Wolsong 2, 3, & 4 using the

PHOENICS2 computer code. It was concluded that steady-state solution could not be achieved and that only a quasi-steady solution could be achieved. It was also reported that a fully converged steady state solution had been obtained when the inlet velocity had been increased by a factor of 1.5 (~3.0 m/s). In this quasi-steady solution, the maximum temperature within the moderator over the period 0~300 s varies between a minimum of 78.5 °C and a maximum of 81.7 °C.

In 1995, Seodijono et al. [3] performed transient moderator analyses after a large reactor inlet header break with or without Class IV power. It was concluded that subcooling remains above 26 °C when Class IV power is available. When Class IV power is not available, the temperature of the top portion of the moderator inside the calandria vessel increases continuously during the post-blowdown phase to reach the saturation temperature.

In the preceding simulations, the CFD moderator analysis model using CFX-4.3 has been validated against 'SPEL moderator circulation experiments', with the maximum error of 2.0 °C.

In this study, a three-dimensional CFD code, CFX-4.3, is used to simulate the moderator circulation inside the calandria vessel under operating conditions. The resultant steady state data will be used as a starting condition for the following transient studies.

2. CANDU6 Moderator System

Figure 2 illustrates the main features of the CANDU 6 moderator system. The calandria vessel is approximately 6.0 m long and 7.6 m in diameter at its widest point. There are 380 calandria tubes which displace about 12 percent of the calandria vessel volume. In addition, there are a number of horizontal and vertical reactivity mechanisms.

The moderator fluid is heavy water. It is extracted from the vessel through two outlet ports located at the bottom of the vessel. The outlet ports are symmetrically located (axially) with respect to the mid-plane perpendicular to the z-axis but are asymmetrically placed towards the moderator pumps in the x-y plane (see Figure 2). After discharging through the outlet ports, the fluid mixes in a header and passes through one of two operating pumps to be cooled via parallel heat exchangers and is returned to the calandria through eight inlet nozzles located at the side of the vessel. The inlet nozzles are symmetrically placed in the x-y plane with respect to the vertical centerline but are asymmetrically placed axially (Figures 2 and 3).

The inlet coolant velocity is of the order of 2 m/s at the nozzle entrance. A front view of the calandria vessel is depicted in Figure 4. The axial locations of the inlet nozzles and outlets are shown in Figure 3.

Under normal operating conditions, nuclear heat generation induces 96.7 MW of power to the moderator fluid. Thus the moderator fluid circulates within the calandria vessel by virtue of a complex interaction of fluid inertia and buoyancy, subject to the influence of a horizontal tube bank.

After leaving the calandria vessel, the heated fluid passes through two parallel heat exchangers. Service water to the heat exchangers is controlled via the Moderator Temperature Control (MTC) program to maintain the calandria moderator outlet temperature at 69.0 °C. Under nominal full power conditions, the corresponding inlet temperature is approximately 45.0 °C.

The total flow rate through the eight nozzles is 940 l/s.

3. Modelling Details and Assumptions

3.1 Assumed Geometry and Problem Definition

The calandria vessel is assumed to be an indented cylinder 6.0 m long with a main-shell diameter of 7.60 m and a sub-shell diameter of 6.76 m. Each of the sub-shells has a length of 0.97 m. Since the sub-shell has a smaller diameter than the main shell, it is necessary to generate two grid blocks; one is a cylindrical-shaped block with a diameter of sub-shell and a length of 6.0 m (block 1), and the other is an annular-shaped block surrounding the other block with a length of 4.0 m (block 2). The volume occupied by in-core devices is not accounted for in this analysis, as it is small compared to the total volume of the calandria tubes.

Fig. 5 shows the multi-block structured grid used in this simulation. The computational grid consisted of 46 angular, 16 radial, and 19 axial divisions in block 1, and of 46 angular, 8 radial, and 15 axial divisions in block 2. The number of total computational cells is 19,504.

The tube bank region is modeled by porous media approach. The hydraulic resistance for the fluid flow in the porous region is accounted for by the momentum source term of governing equations using empirical correlations. The detailed procedure will be presented in the next section. The calandria tube pitch is 0.286 m and the calandria tube diameter is 0.131 m. The diameter of the core region is 6.292 m, so the volume porosity γ of assumed porous media becomes 0.8357.

The Boussinesq approximation in which density is a linear function of temperature is used to model buoyancy forces. The standard k- ϵ turbulence model associated with logarithmic wall treatment is used, as the flow field is known to be turbulent.

At 100% full power, the total heat load to the moderator is estimated to be 96.7 MW consisting of 90.8 MW to the core region and 5.9 MW to the reflector region. For conservatism, the total heat load to the moderator is taken to be 103 MW consisting of 96.7 MW to the core and 6.3 MW to the reflector region. This increased heat load corresponds to 103% full power. The total inlet nozzle flow rate is taken to be the design value of 940 l/s. This flow rate is assumed to be equally distributed to each of the eight inlet nozzles, i.e., 117.5 l/s per nozzle.

The working fluid is heavy water at 1 atm. The properties are set as uniform and constant. The wall boundary condition is not set to be adiabatic, in order to simulate the real situation. Thus, a small amount of heat transfer through the circumferential wall is allowed. From the rough evaluation of natural convection from horizontal cylinders(Chap. 7 of [7]), the heat transfer coefficient of the calandria outer wall is 200.0 ~ 500.0 W/m²C for the temperature difference of 0.5 ~ 4.0°C between the wall and the fluid. In this simulation, the wall boundary condition is set to be the constant heat flux of -300.0 W/ m²C.

The close two inlet nozzles are merged into one solid patch and a surface patch in the grid(Fig. 5), so that only the nozzle end parts appear in the grid with the size of 2x2x5 (IxJxK) cells. The inlet velocity is ~2.0 m/s at the angle of 14° from the vertical direction, which corresponds to the total mass flow rate of 940 l/s with the given inlet nozzle area and fluid density. The inlet fluid temperature is 45 °C (318 °K), with a total heat load of 103 MW.

3.2 Hydraulic Resistance for the Flows in the Porous Media

To avoid the complexity of generating grids around every heating tube, the porous media approach is

applied in the current study. The momentum equation is expressed in the CFX-4.2 manual [5] as

$$\frac{\partial \rho \mathbf{U}}{\partial t} + \nabla \cdot (\rho \mathbf{U} \otimes \mathbf{U}) = \mathbf{B} + \nabla \cdot \boldsymbol{\sigma} \quad (1)$$

Here, \mathbf{B} has units of force per unit volume, (N/m^3) in SI units. The hydraulic resistance (impedance) of the porous region is put as a function of local velocity using the subroutines provided by CFX-4.3.

$$\mathbf{B} = \mathbf{B}_o + \mathbf{B}_p \mathbf{U} \quad (2)$$

where \mathbf{B}_o is velocity-independent body force. \mathbf{B}_p (Ns/m^4) is useful to assign flow resistance depending on the local velocity. For an an-isotropic porous region, $\mathbf{B} = -\mathbf{R}\mathbf{U}$, with $\mathbf{R} = \text{diag}(R_x, R_y, R_z)$.

For axial flow, there is no form drag. The value of R_z may be expressed as below (reference[6]):

$$R_z = \frac{\Delta p_{fric}}{\Delta z} = \frac{f}{D_e} \cdot \frac{\rho u_z}{2} \quad (3)$$

where f is the friction factor and D_e is the hydraulic diameter of flow passage in z-direction.

Hadaller et al.[4] investigated the frictional pressure drop for staggered and in-line tube banks, in which the Reynolds number range is 2000 to 9000 and pitch to tube diameter ratio is 2.16. Also, they concluded that for the given p/d ratio the effect of staggering is not important. In our study, the tube Reynolds number is around 2000 and p/d ratio is 1.974. Applying the conclusion of Hadaller et al.[4], the resistances depending on the local velocity for transverse flow to the tube matrix are expressed by the correlation below.

$$R_i = \frac{f}{2} \rho \gamma |\mathbf{V}|, \quad i = x, y \quad (4)$$

where the quantity $|\mathbf{V}|$ is the local magnitude of time-mean fluid velocity, u_i is a velocity component, and f is a loss factor determined from an empirical equation for the losses through tube bundle regions. The ratio of fluid volume to the total volume in the porous region is defined as the volume porosity γ . The 1990 Stern lab experiments suggest,

$$f = 4.5626 \frac{\text{Re}^{-0.1655}}{P \gamma^2 R_f} \quad (5)$$

where Re is the Reynolds number = $\gamma |\mathbf{V}| D_{\text{tube}} / \nu$, D_{tube} is the diameter of the calandria tubes, ν is the kinematic viscosity of the fluid, P is the distance between calandria tube centerlines (pitch), and R_f is a friction coefficient reduction factor that ranges between 0.12 and 1.0 depending on the flow attack angles to the calandria tubes.

4. Simulation Results

This steady state computation using CFX-4.3 was performed in an HP-C3600 workstation. The convergence criteria were the enthalpy residual reduction factor of 10^4 and the largest mass residual of 10^{-5} . Because the energy equation and momentum equations are strongly interrelated in this computation, the algebraic multi-grid solver and false time stepping technique were adapted to accelerate converging speed for the

energy equation. The number of steady computation iterations was about 60,000~80,000.

The resultant velocity field and temperature distribution is presented in 5 slices of constant z and 1 slice of constant x . The z values of constant- z -slices were selected carefully. Therefore, two slices include inlet nozzles and an outlet(Fig. 6 & 10), and the other two slices include inlet nozzles only(Fig. 7 & 9). The last slice contains no nozzle but also outlets(Fig. 8), which represents the x - y plane between the inlets. The x value of constant- x -slice is 0.5.

Fig. 6 shows the velocity vectors and temperature contours in the x - y plane of $z = 1.418$ m, where each inlet nozzle and outlet are cut through. In Fig. 6(a), the cold injected fluid through the inlet nozzles changes its direction downward due to the suppression of hot fluid from the top of the calandria vessel. The reversed fluid goes down to the bottom, guided by the circumferential lower vessel wall. Most of these cold fluids at the bottom go out through the outlet, while some go up into the vacancy that is created by the elevation of heated fluid inside the porous region. Inside the central porous region, the elevation speed of hot fluid induced by buoyancy forces is relatively slow because of the hydraulic resistance. In Fig. 6(b), temperature distribution shows a steep change of temperature around the jet reversal area, where cold fluid from the inlet jet and hot fluid from the top meet together. Along the lower circumferential vessel wall, the lowest temperature area exists. At the central area, there exists a hot region just below the center where the temperature is higher than 355 K. The highest temperature region($T > 360$ K) is located at the top of the calandria vessel.

Fig. 7 shows the velocity vectors and temperature contours in the x - y plane of $z = 2.2$ m, where only the inlet nozzles are cut. In Figure 7(a), jet reversal flows also appear in this plane, but there is no large exiting velocity vector. In Figure 7(b), the temperature contour trend is almost the same as Figure 6(b), except that the area of the hot region($T > 355$ K) at the lower center is smaller than that of Figure 6(b).

Fig. 8 represents the velocity field and temperature distribution in the x - y plane of $z = 2.935$ m, the exact intermediate plane between two nozzles' locations. There is no inlet jet in this plane. Thus, the heated fluids from the top go all the way down toward the bottom of the calandria vessel, guided by the circumferential wall. The temperature distribution of this plane shows a smaller hot region ($T > 355$ K) at the lower center.

Figures 9 and 10 represent resultant velocity fields and temperature distributions in the x - y planes of $z = 4.0$ m and $z = 4.582$ m, respectively. Overall trends are similar to those of Figs. 7 and 6. Due to the asymmetry across the central x - y plane, the flow rates of each outlet are not the same. The velocity fields and temperature distributions of Figures 6 and 10 show slight differences from each other.

Fig. 11 shows the velocity vectors and temperatures in the y - z plane of $x = 0.5$ m. From Figure 11(a), it is shown that there is no large fluid movement in the z -direction around the center region. The heated fluids at the top of the sub-shell go into the top portion of the main-shell. Near the outlets at the bottom of the main-shell, fluids go toward the closer outlet with relatively large speeds. Note that the vector length is increased to present relatively smaller velocity vectors clearly. In Figure 11(b), the isotherms at the lower part of the vessel indicate that the fluids in these areas are stratified. At the central area and upper area, the isotherms show the shape of upward convex.

5. Conclusions

In this study, the CANDU moderator analysis model using CFX-4.3 is established and the simulation for

predicting local subcooling of the moderator in the vicinity of calandria tubes in the CANDU reactor is performed. The temperature distributions and velocity fields of the simulation results are presented. With 103% full power for conservatism, the maximum temperature of the moderator is 363.3 K (90.3 °C) and is located at the top of the calandria vessel. Therefore, the minimum subcooling evaluated is 17.4 °C, conservatively.

Acknowledgement

This study has been carried out as a part of the CANDU Safety Analysis System Establishment program supported by Korea Ministry of Science & Technology.

References

1. D. Koroyannakis, R.D. Hepworth, G. Hendrie, "An Experimental Study of Combined Natural and Forced Convection Flow in a Cylindrical Tank," TDVI-382, AECL, Dec.1983.
2. W.M. Collins, "PHOENICS2 Model Report for Wolsong 2/3/4 Moderator Circulation Analysis," Wolsong NPP 2/3/4, 86-03500-AR-053, Revision 0, 1995.
3. P. Seodijono, W.M. Collins, and T. De, "Moderator Analysis for In-Core and Out-of-Core Loss of Coolant Accident (LOCA)," Wolsong NPP 2/3/4, 86-03500-AR-052, Revision 0, 1995.
4. G.I. Hadaller, R.A. Fortman, J. Szymanski, W.I. Midvidy and D.J. Train, "Frictional Pressure Drop for Staggered and In Line Tube Bank with Large Pitch to Diameter Ratio," Preceedings of 17th CNS Conference, Fredericton, New Brunswick, Canada, June 9-12, 1996.
5. *CFX-4.2: Solver Manual*, CFX International, United Kingdom, December 1997.
6. N.E. Todreas and M.S. Kazimi, *Nuclear System II: Elements of Thermal Hydraulic Design*, Chap.5, Hemisphere Publishing Corporation, 1990.
7. J.P. Holman, *Heat Transfer*, 6th ed., Chap. 7, McGraw-Hill, 1986

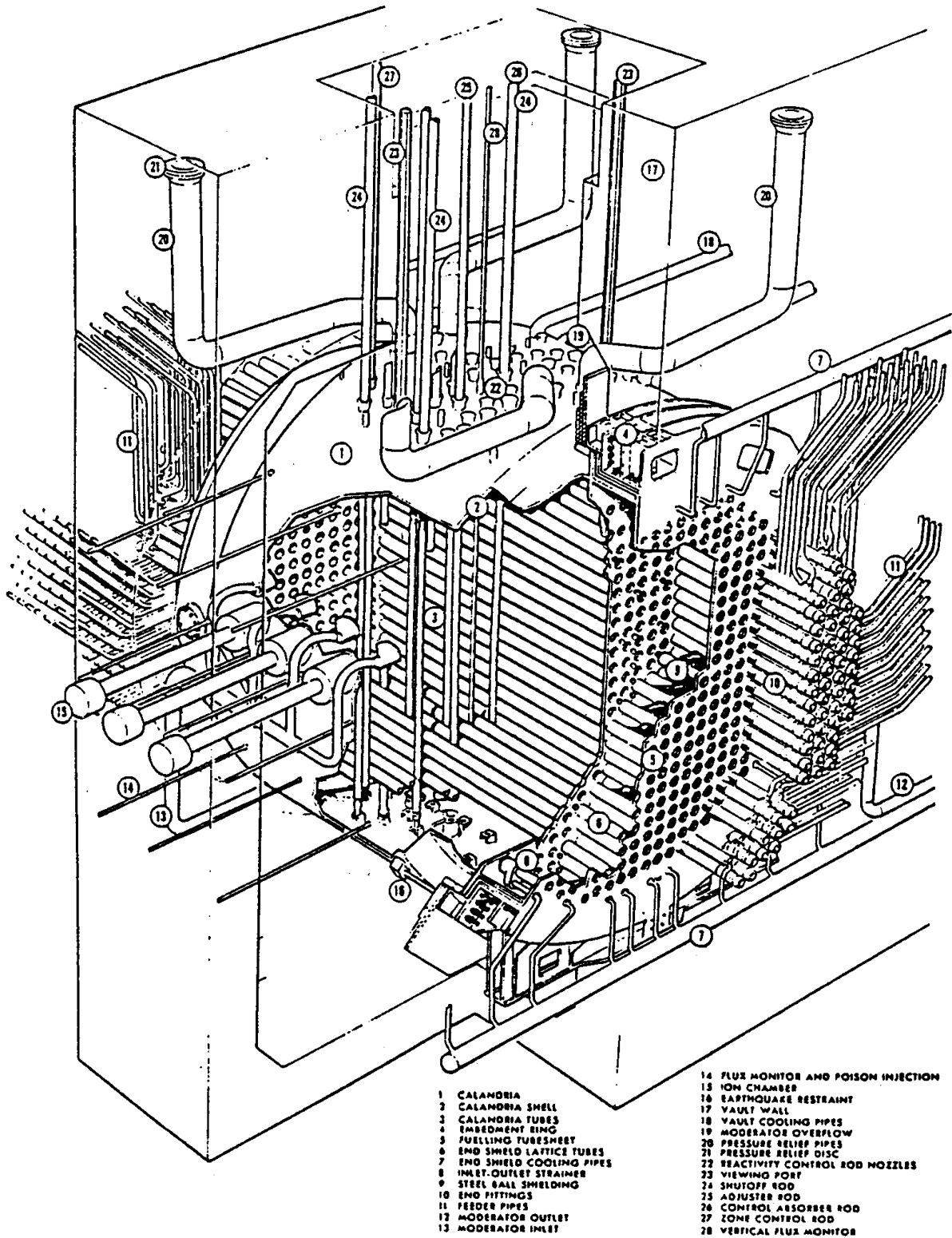


Fig. 1 CANDU reactor assembly

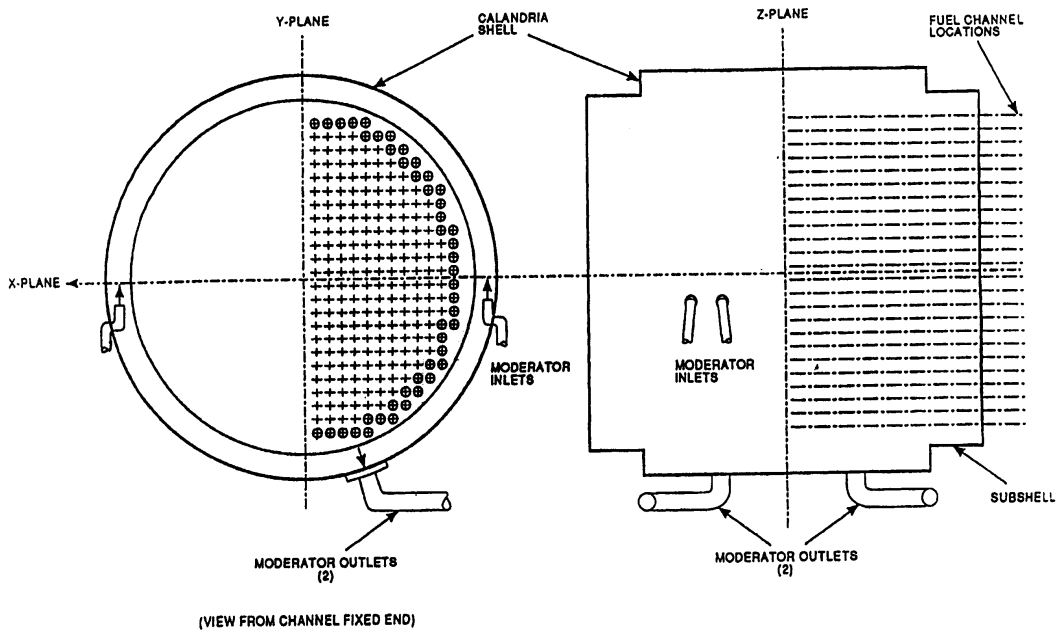


Fig. 2 CANDU6 Moderator System

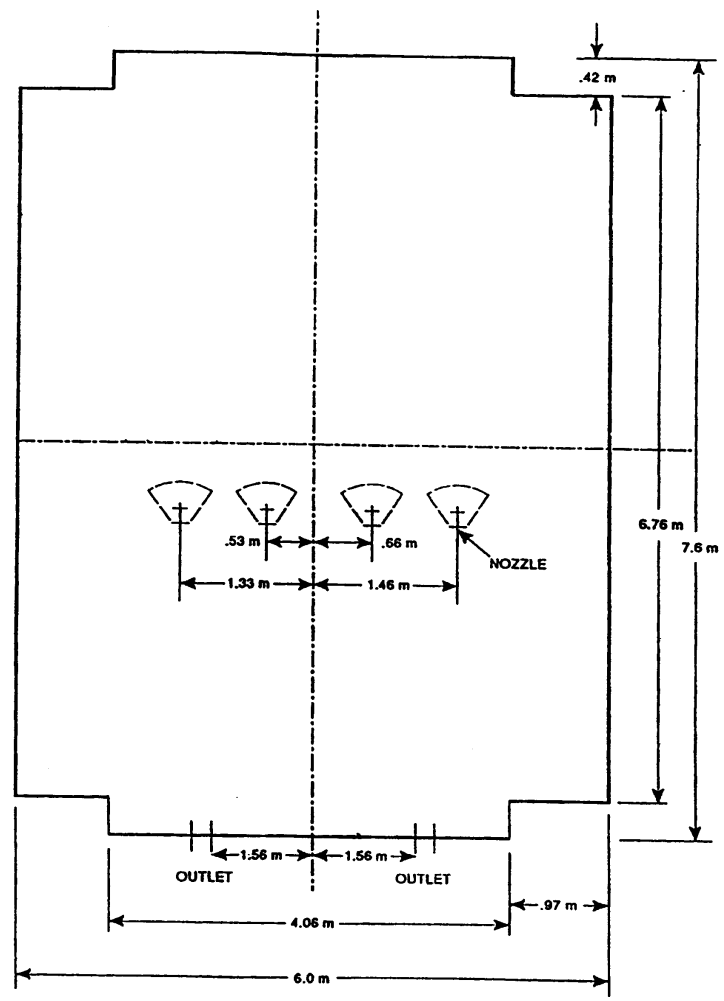


Fig. 3 Calandria Vessel Side View

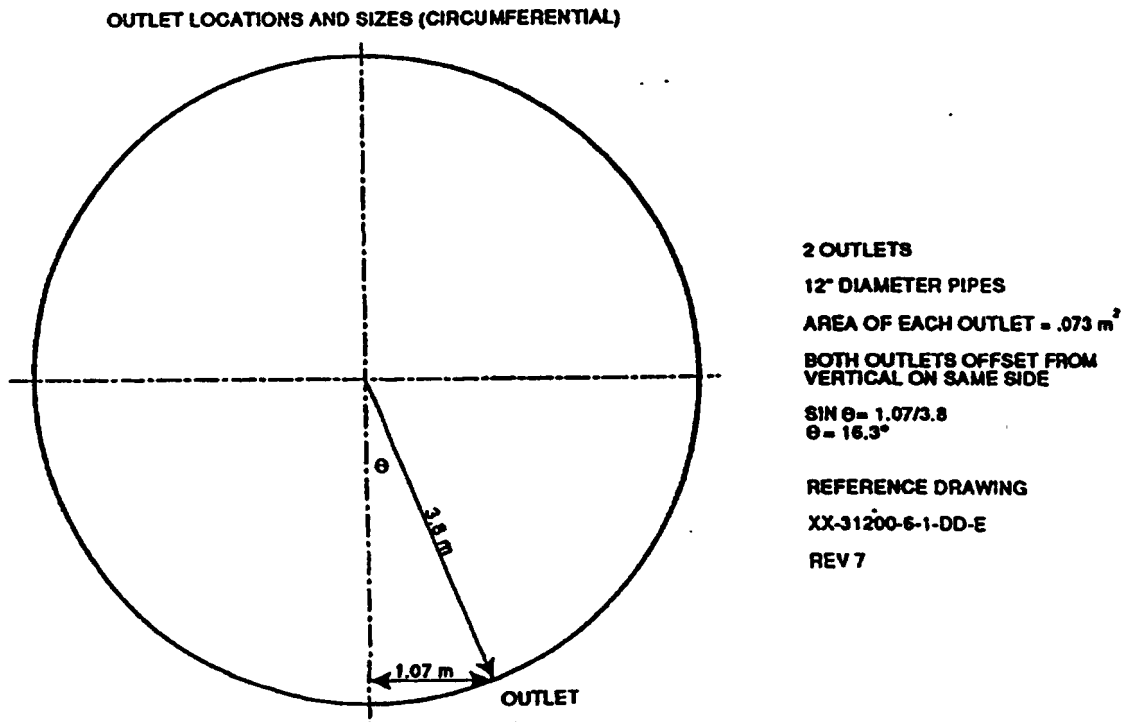
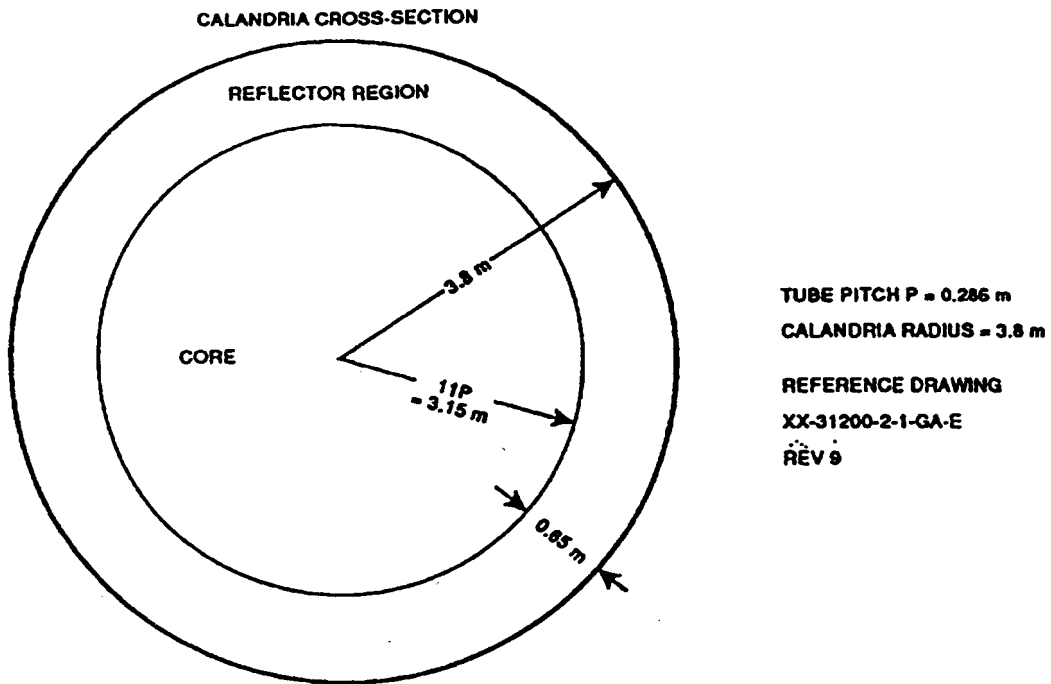


Fig. 4 Relevant Calandria Dimensions and Location of Outlets

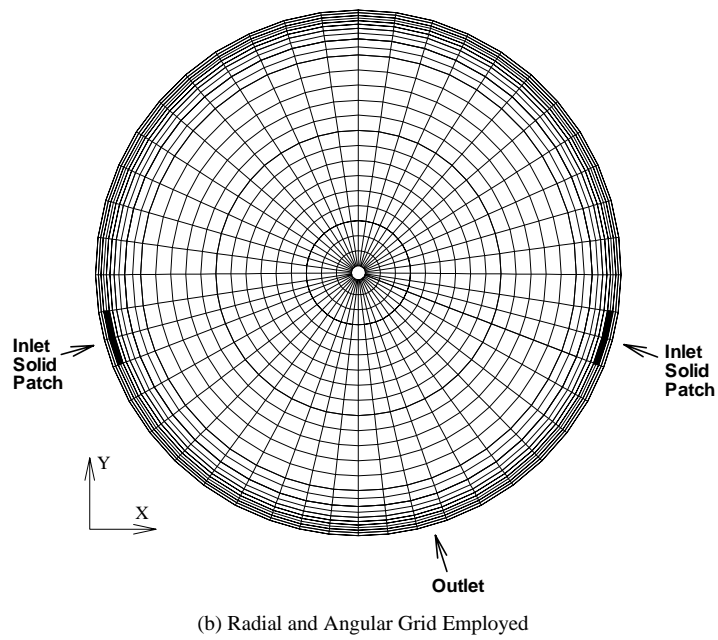
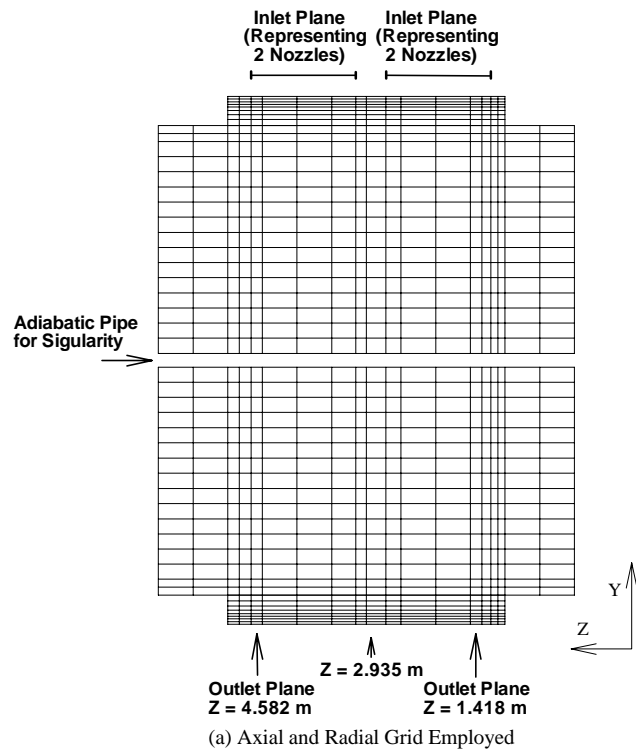


Fig. 5 3-D Grid Employed in Current Simulation

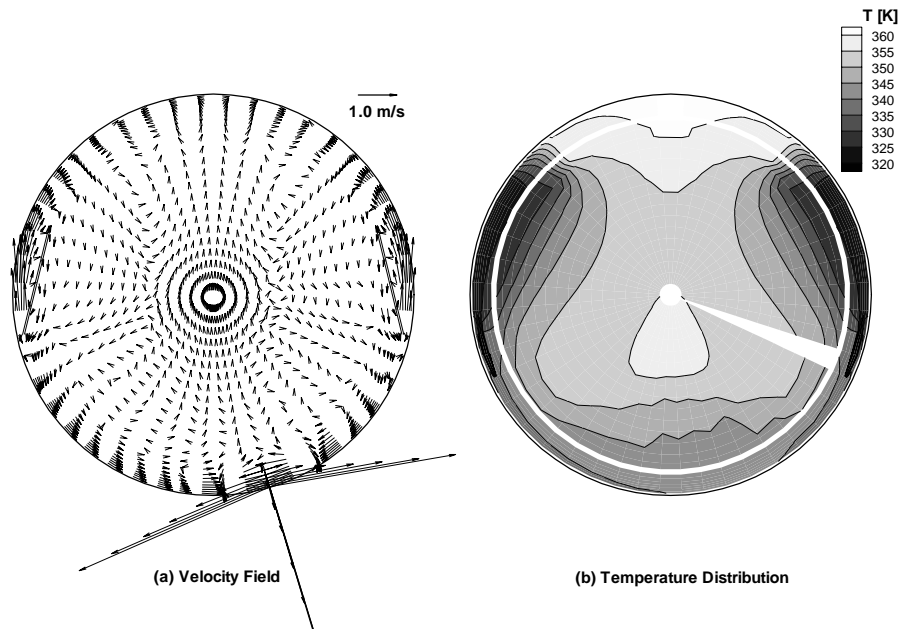


Fig. 6 Velocity Field and Temperature Distribution at $Z=1.418$ m, from Current Simulation

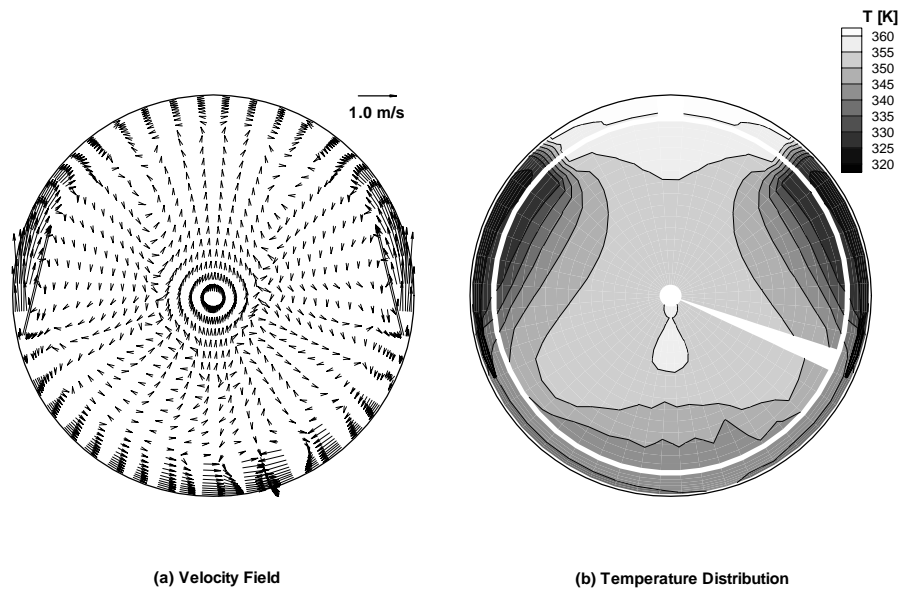


Fig. 7 Velocity Field and Temperature Distribution at $Z=2.2$ m, from Current Simulation

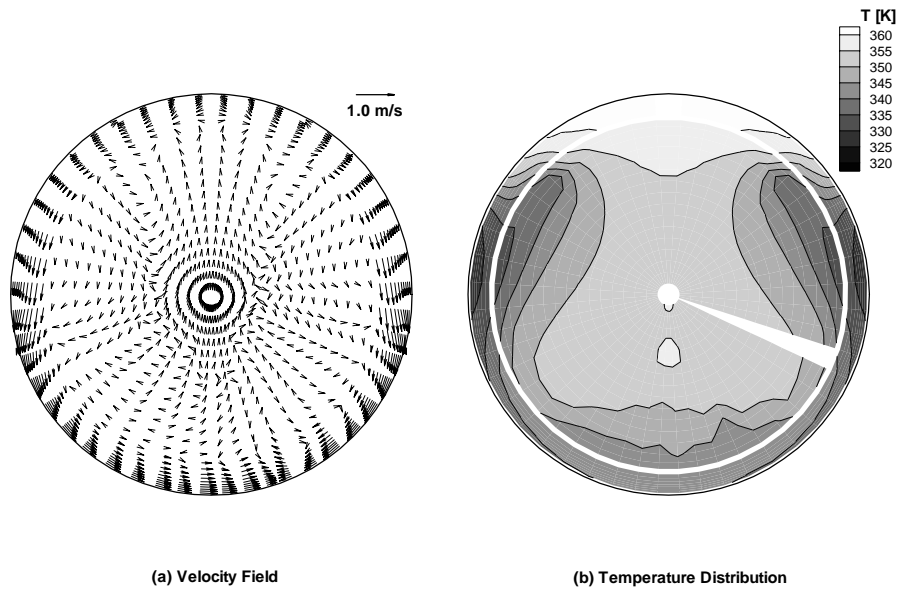


Fig. 8 Velocity Field and Temperature Distribution at $Z=2.935$ m, from Current Simulation

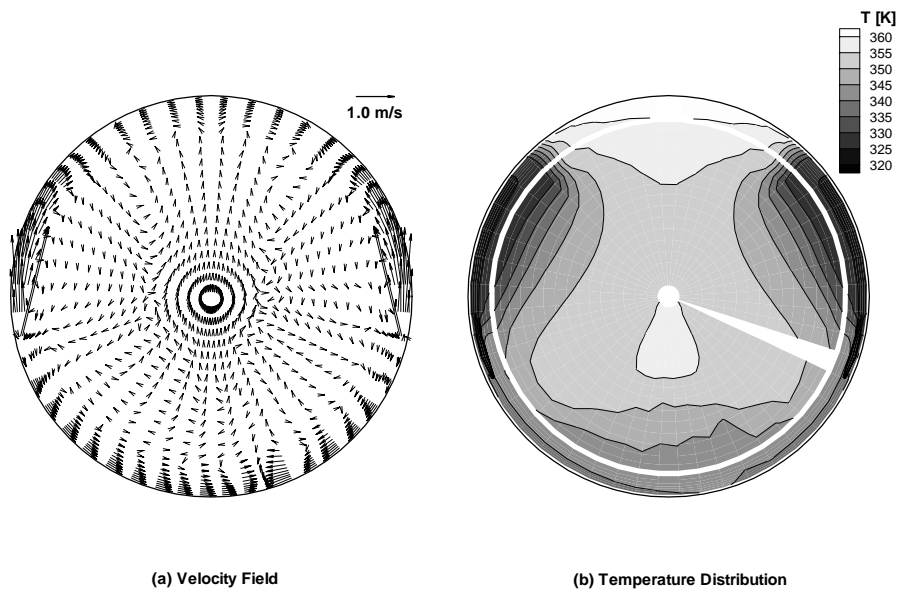


Fig. 9 Velocity Field and Temperature Distribution at $Z=4.0$ m, from Current Simulation

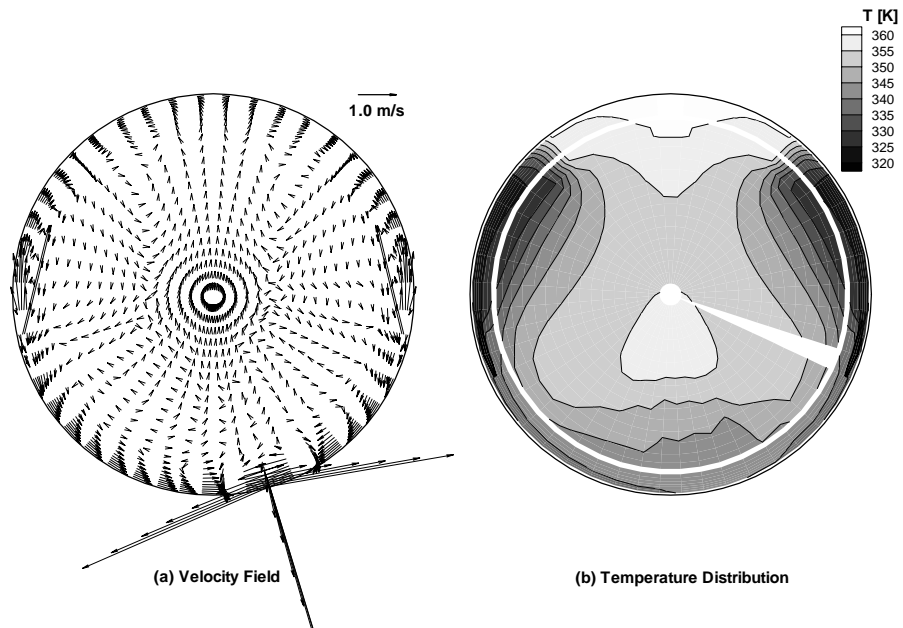


Fig. 10 Velocity Field and Temperature Distribution at $Z=4.582$ m, from Current Simulation

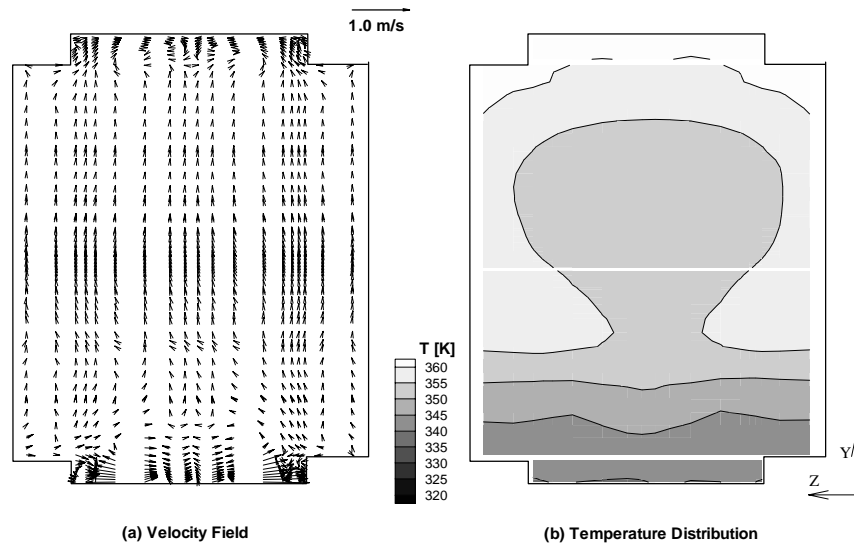


Fig. 11 Velocity Field and Temperature Distribution at $X=0.5$ m, from Current Simulation